Enhanced magnon spin transport in NiFe2O4 thin films on a lattice-matched substrate

Shan, J.; Singh, A. V.; Liang, L.; Cornelissen, L. J.; Galazka, Z.; Gupta, A.; van Wees, B. J.; Kuschel, T.

Published in:
Applied Physics Letters

DOI:
10.1063/1.5049749

Publication date:
2018

Enhanced magnon spin transport in $NiFe_2O_4$ thin films on a lattice-matched substrate

Cite as: Appl. Phys. Lett. **113**, 162403 (2018); https://doi.org/10.1063/1.5049749
Submitted: 25 July 2018 . Accepted: 29 September 2018 . Published Online: 16 October 2018

J. Shan, A. V. Singh, L. Liang, L. J. Cornelissen, Z. Galazka, A. Gupta, B. J. van Wees, and T. Kuschel

Enhanced magnon spin transport in $NiFe_2O_4$ thin films on a lattice-matched substrate

J. Shan,[1,a)] A. V. Singh,[2] L. Liang,[1] L. J. Cornelissen,[1] Z. Galazka,[3] A. Gupta,[2] B. J. van Wees,[1] and T. Kuschel[1,4]

[1]*Physics of Nanodevices, Zernike Institute for Advanced Materials, University of Groningen, Nijenborgh 4, 9747 AG Groningen, The Netherlands*

[2]*Center for Materials for Information Technology, The University of Alabama, Tuscaloosa, Alabama 35487, USA*

[3]*Leibniz Institute for Crystal Growth, Max-Born-Str. 2, 12489 Berlin, Germany*

[4]*Center for Spinelectronic Materials and Devices, Department of Physics, Bielefeld University, Universitätsstraße 25, 33615 Bielefeld, Germany*

(Received 25 July 2018; accepted 29 September 2018; published online 16 October 2018)

We investigate magnon spin transport in epitaxial nickel ferrite ($NiFe_2O_4$, NFO) films grown on magnesium gallate spinel ($MgGa_2O_4$, MGO) substrates, which have a lattice mismatch with NFO as small as 0.78%, resulting in the reduction of antiphase boundary defects and thus in improved magnetic properties in the NFO films. In nonlocal transport experiments where platinum (Pt) strips function as magnon spin injectors and detectors, enhanced signals are observed for both electrically and thermally excited magnons, and the magnon relaxation length (λ_m) of NFO is found to be around 2.5 μm at room temperature. Moreover, at both room and low temperatures, we present distinct features from the nonlocal spin Seebeck signals which arise from magnon-polaron formation. Our results demonstrate excellent magnon transport properties (magnon spin conductivity, λ_m, and spin mixing conductance at the Pt/NFO interface) of NFO films grown on a lattice-matched substrate which are comparable with those of yttrium iron garnet. *Published by AIP Publishing.*
https://doi.org/10.1063/1.5049749

Magnons, the collective excitation of spins, are playing the central role in the field of insulator spintronics.[1] Magnons in magnetic materials can interact with conduction electrons in adjacent heavy metals, transferring spin angular momentum and thus allowing for magnonic spin current excitation and detection using electrical methods.[2–9] Besides, magnons can be driven thermally, known as the spin Seebeck effect (SSE).[10–12] Both magnons generated by a spin voltage bias and a temperature gradient can be transported for a certain distance on the order of a few to tens of micrometers, as reported recently in ferrimagnetic[2,13] and even in antiferromagnetic materials,[14] making magnons promising candidates as information carriers.

Nickel ferrite (NFO) is a ferrimagnetic insulator with an inverse spinel structure. It is widely used in high-frequency systems in conventional applications.[15] Recently, NFO and other spinel ferrites were explored for spintronic applications, where effects such as spin Hall magnetoresistance (SMR),[16–20] SSE,[21–28] and nonlocal magnon spin transport[13] were reported. In most of these studies, large magnetic fields of a few teslas are required to align the magnetization of the ferrites, possibly due to the presence of antiphase boundaries.[29]

However, it was recently shown that the NFO films grown on nearly lattice-matched substrates with similar spinel structures, such as $MgGa_2O_4$ and $CoGa_2O_4$, exhibited superior magnetic properties due to the elimination of antiphase boundaries, leading to, for instance, a larger saturation magnetization (M_S), smaller coercive fields, and a lower Gilbert damping constant, compared to the NFO films grown on the typically used $MgAl_2O_4$ (MAO) substrate.[30] An enhanced longitudinal SSE effect was reported on such NFO films.[31] It can be expected that the nonlocal transport properties of magnon spin are also elevated in these NFO films, as we discuss in this paper.

We studied two NFO films on MGO (100) substrates, with thicknesses of 40 nm and 450 nm, respectively. NFO films were grown by pulsed laser deposition, in the same way as described in Refs. 30 and 31. Prior to further processes, the 450-nm-thick sample was characterized by superconducting quantum interference device (SQUID) magnetometry, exhibiting an in-plane coercive field lower than 5 mT [see Fig. 1(b)]. Afterwards, multiple devices were fabricated on both samples. Figure 1(a) shows schematically the typical geometry of a device, where two identical Pt strips serving as magnon spin injectors and detectors are patterned in parallel with a center-to-center spacing d, ranging from 0.3 to 25 μm for all devices. The lengths and widths of the Pt strips are designed to be different for shorter- and longer-d devices, as summarized in Table I. In Geometry I, Pt strips are 100 nm in width, allowing for fabrication of devices with narrow spacings. In Geometry II, Pt strips are wider and longer, permitting larger injection currents which yield a larger signal-to-noise ratio, so that small signals can be resolved. For all devices, Pt is sputtered with a thickness of 8 nm, showing a conductivity of around 3×10^6 S/m. Contacts consisting of Ti (5 nm)/Au (60 nm) were patterned in the final step of device fabrication.

Electrical measurements were performed with a standard lock-in technique, where a low-frequency ac current, $I = \sqrt{2} I_0 \sin(2\pi f t)$, was used as the input to the device, and

a)j.shan@rug.nl

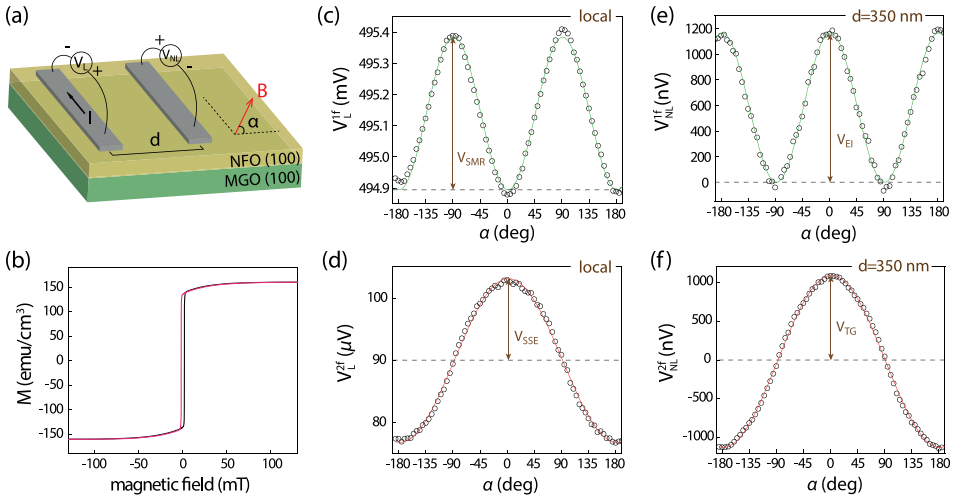

FIG. 1. (a) Schematic geometry of local and nonlocal measurements. An electric current I is applied at one Pt strip, and voltages can be detected at the same strip (locally) or at the other one (nonlocally). An in-plane magnetic field is applied at an angle denoted by α. (b) In-plane magnetization of the 450 nm-thick NFO film obtained from SQUID at room temperature. (c)–(f) Room-temperature local and nonlocal measurements shown in first and second harmonic signals, with $I = 100\,\mu$A. They are measured on the 40-nm-thick NFO sample with an external magnetic field of 300 mT under angular sweep. Only for (e), a background of 910 nV is subtracted.

voltage outputs were detected at the same ($1f$) or double frequency ($2f$), representing the linear and quadratic effects, respectively. In this study, typically I_0 is 100 μA and f is set to be around 13 Hz. For the local detection V_L, as shown in Fig. 1(a), V_L^{1f} detects the resistance and magnetoresistance (MR) effect of the Pt strip, and V_L^{2f} incorporates the current-induced local SSE.[32,33] For the nonlocal detection V_{NL}, V_{NL}^{1f} represents the nonlocal signals from magnons that are injected electrically via SHE,[2,3] and V_{NL}^{2f} stands for the nonlocal SSE.[2,13,34–38] The conductance of the NFO thin films was checked by measuring resistances between random pairs of electrically detached contacts, which yielded values over GΩ, confirming the insulating nature of the NFO films.

We first perform angular-dependent measurements at room temperature for both local and nonlocal configurations, with results plotted in Figs. 1(c)–1(f). The sample was rotated in-plane with a constant magnetic field applied. The strength of the field is 300 mT, large enough to saturate the NFO magnetization along the field direction. A strong MR effect, with $\Delta R/R \approx 0.1\%$, was observed from the local V_L^{1f} signal [see Fig. 1(c)]. This MR effect was checked to be magnetic-field independent in the range from 100 to 400 mT, indicating that the observed MR effect is the SMR effect which is sensitive to the NFO magnetization that is saturated in this range, instead of the Hanle MR effect[39] which depends on the external magnetic field. This is in marked contrast to the previous observations from sputtered NFO thin films grown on MAO, where only the Hanle MR effect was observed at fields above 1 T.[13] The SMR ratios for both 40- and 450-nm thick samples exhibit similar values, ranging between 0.07% and 0.1%, around 3 to 4 times larger than those for Pt/yttrium iron garnet (YIG) systems with a similar Pt thickness.[6,34,40] It is also more than twice as large as the SMR reported from Pt/NFO systems with the NFO layer grown by chemical vapor deposition on MAO substrates.[17] Using the average SMR ratio of 0.08% and the spin Hall angle of Pt of 0.11,[6,34] we estimated the real part of the spin mixing conductance (G_r) for Pt/NFO systems to be 5.7×10^{14} S/m^2 with the SMR equation,[41] being more than 3 times larger than that of the Pt/YIG systems determined with the same method.[6]

TABLE I. Sample details of Geometry I and II.

Geometry	Pt length (μm)	Pt width (μm)	distances (μm)
I	10	0.1	0.3–2
II	20	0.5	2–25

Figures 1(e) and 1(f) plot typical results from the nonlocal measurements in V_{NL}^{1f} and V_{NL}^{2f}, showing $\cos^2(\alpha)$ and $\cos(\alpha)$ dependences, respectively, the same as observed previously in YIG or NFO films with Pt or Ta electrodes.[2,13,34,42,43] For the magnon transport process represented by V_{NL}^{1f}, both the magnon excitation and detection efficiencies are governed by $\cos(\alpha)$, which in total yields a $\cos^2(\alpha)$ behavior. For V_{NL}^{2f}, on the other hand, the thermal magnon excitation is independent of α but the detection process is, thus showing a $\cos(\alpha)$ dependence. Their amplitudes, denoted as V_{EI} and V_{TG}, respectively, can be obtained from sinusoidal fittings.

Next, we present V_{EI} and V_{TG} for all devices as a function of d on both the 40- and 450-nm-thick samples to investigate the magnon relaxation properties, as shown in Fig. 2. For both V_{EI} and V_{TG}, discontinuities are found between Geometries I ($d \leq 2\,\mu$m, filled with yellow color) and II ($d \geq 2\,\mu$m), even though the data from Geometry II are carefully normalized to Geometry I as was done for Pt/YIG nonlocal devices to link the data between the two geometries.[34] However, this normalization method is based on the assumption of noninvasive contacts and does not account for the additional spin absorption that was induced by widening the Pt contact width. This normalization method works well for Pt/YIG systems but becomes less satisfactory for Pt/NFO systems as we study here, which is expected in view of a larger G_r value.

For V_{EI}, the datapoints at $d > 15\,\mu$m ($d > 12\,\mu$m for 450 nm NFO) are not plotted as the signal amplitudes become much smaller than the noise level. For shorter distances ($d < 1\,\mu$m), the signals on both samples are even comparable to those measured on thin YIG films with similar device geometry,[2,34] although a fairer comparison should be made with the same thickness of the magnetic insulators. We can also make a comparison between the V_{EI} signals from the 40-nm-thick NFO film studied here and the 44-nm-thick sputtered NFO film on the MAO substrate studied in Ref. 13. We found that for the same device geometry ($d = 350$ nm)

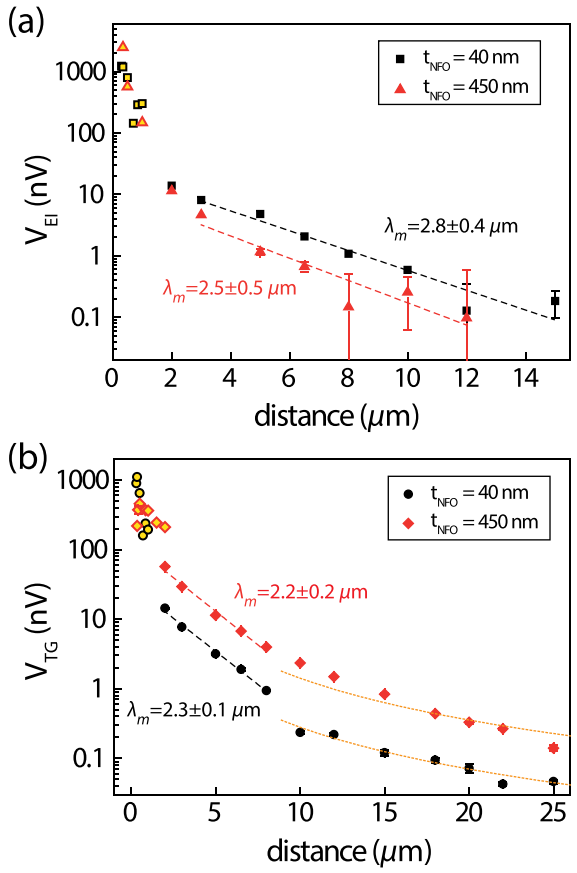

FIG. 2. Distance dependence of (a) V_{EI} and (b) V_{TG} measured at B = 200 mT on both NFO samples at room temperature, normalized to $I = 100$ μA. The datapoints filled with yellow color are obtained from devices in Geometry I, while the rest belongs to Geometry II. The datapoints from Geometry II are normalized to Geometry I as described in Ref. 34 for better comparison. Dashed lines are exponential fittings with the formula $V = A\exp(-d/\lambda_m)$, with the coefficient A being different for each fitting. The extracted λ_m from each fitting is indicated nearby. The dotted orange lines in (b) are $1/d^2$ fittings for long-d results.

and Pt thickness, the V_{EI} signal amplitudes obtained here are around 100 times larger than found in Ref. 13, showing the superior quality of the NFO films studied in this paper.

To extract λ_m for these NFO samples at room temperature, we performed exponential fittings as shown in Fig. 2(a) by the dashed lines. We limit the fit to the datapoints in the exponential regime where $d > 2$ μm. Both datasets yield $\lambda_m \approx 2.5$ μm for the two NFO samples with different thicknesses. It is noteworthy that the V_{EI} signals for the 450 nm NFO are in general smaller than those for the 40 nm NFO sample, except for one datapoint at the shortest distance. However, one would expect the opposite, as increasing the NFO thickness from 40 to 450 nm enlarges the magnon conductance without introducing an extra relaxation channel vertically, given that 450 nm is still much smaller than $\lambda_m \approx 2.5$ μm. This puzzle is similar to that for Pt/YIG systems,[34] and the reason is not yet clear to us.

Now, we move to the thermally generated nonlocal SSE signals V_{TG} as shown in Fig. 2(b). According to the bulk-generated SSE picture,[6,34,38,44] at a certain distance (d_{rev}), V_{TG} should reverse sign, where in short distances V_{TG} has the same sign as the local SSE signal, and further away, the sign alters. d_{rev} is influenced by the thickness of the magnetic insulator and interfacial spin transparency at the contacts.[34] With our measurement configuration [the polarities of local and nonlocal measurement configurations are opposite as shown in Fig. 1(a)], the V_{TG} signals measured from all devices are in fact opposite in sign compared to the local SSE signals [see Fig. 1(d)], meaning that d_{rev} is positioned closer than the shortest d we investigated. Only an upturn is observable for V_{TG} of the 450 nm NFO sample in a short-d range. Compared to Pt/YIG systems, where d_{rev} is about 1.6 times of the YIG thickness, for Pt/NFO systems, the sign-reversal takes place much closer to the heater, possibly because of the Pt/NFO interface being more transparent for a larger G_r.

Exponential fittings can also be carried out for V_{TG} on both samples. Note that only the datapoints in the exponential regime can be used to extract λ_m, which typical starts at $d = \lambda_m$ and extends to a few λ_m.[36] Further than the exponential regime, V_{TG} starts to decay geometrically as $1/d^2$, dominated by the temperature gradient present near the detector. Based on λ_m that we extracted from the decay of the electrically injected magnon signals, we identify $2 \le d \le 8$ μm as the exponential regime and obtain λ_m to be around 2.2 or 2.3 μm from the decay of V_{TG}. The consistency between λ_m found from magnon signals excited electrically and thermally illustrates again the same transport nature of the magnons generated in both methods.

Owing to the excellent quality of the NFO films, we are able to study their magnetoelastic coupling by means of the nonlocal SSE. It was observed in YIG that for both the local and nonlocal SSE signals, spike structures arose at certain magnetic fields, at which the magnon and phonon dispersions became tangent to each other, resulting in a maximal magnetoelastic interaction and the formation of magnon-polarons.[38,45–48] At these conditions, the spin Seebeck signals have extra contributions from the magnon-polarons, provided that the magnon and phonon impurity scattering potentials are different.[45,46] It was found that for YIG films, the acoustic quality is higher than the magnetic one, with *peaks* observed in local SSE and nonlocal SSE ($d < d_{rev}$) measurements and *dips* observed for nonlocal SSE where $d > d_{rev}$.[38,45] This effect is explained as several parameters such as λ_m, the bulk spin Seebeck coefficient, the magnon spin, and heat conductivities are all modified by the emergence of magnon-polarons.[38,46] So far, this resonant enhancement/suppression of SSE caused by magnetoelastic coupling has only been clearly observed in YIG; besides, a bimodal structure was found in the SSE of a $Ni_{0.65}Zn_{0.35}Al_{0.8}Fe_{1.2}O_4$ thin film and was speculated to be related to magnon-phonon interactions.[49]

Here, we present distinctive magnon-polaron features in the nonlocal SSE measurements on our NFO films. Figure 3 shows field-sweep data of V_{TG} performed on one device of the 450-nm-thick NFO sample at $T = 150$ K and 293 K. At both temperatures, asymmetric dip structures of V_{TG} are clearly visible, around ±4.2 T at $T = 150$ K, and shift to ±4.0 T at $T = 293$ K. The change in the characteristic magnetic field of 0.2 T for a temperature decrease of about 150 K is comparable to Pt/YIG systems.[38] The sign of the anomalies is in accordance with the previous observation reported in Ref. 38, considering that the spacing between the Pt strips ($d = 1$ μm) is further than d_{rev}. This implies that the studied NFO film may also have a higher acoustic than magnetic

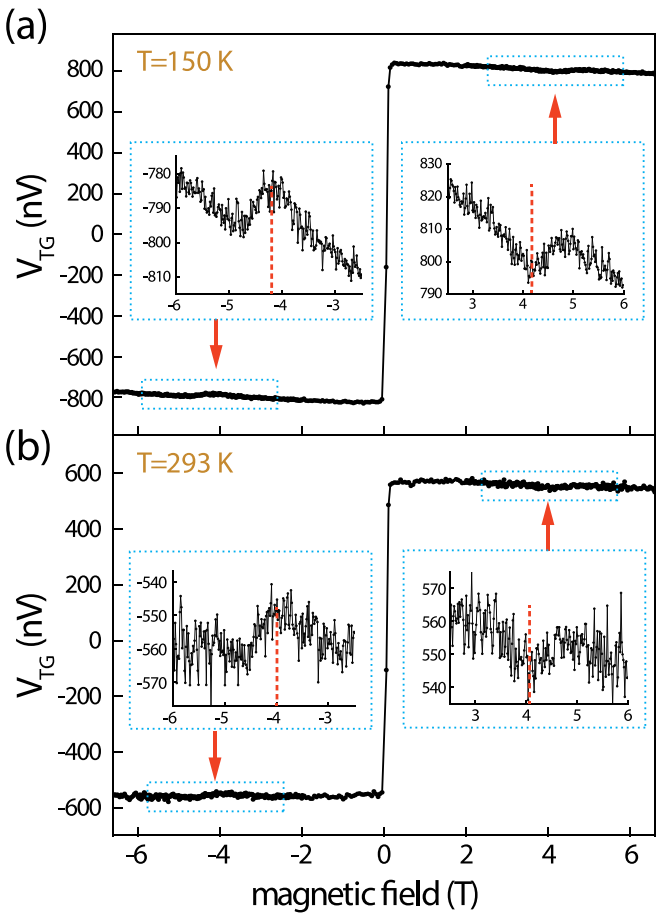

FIG. 3. Magnetic field sweep measurements of V_{TG} at (a) $T = 150$ K and (b) $T = 293$ K, on the 450 nm NFO sample ($d = 1\,\mu$m) from the nonlocal spin Seebeck measurements with $\alpha = 0°$. Insets show close-ups of the resonant dips.

quality like YIG, although a careful study which measures the anomalies from the local SSE is needed.

The magnetic fields where the anomalies occur can be evaluated by the phonon and magnon dispersions. In our experiments, limited by the maximal applied magnetic field ($\mu_0 H \approx 7$ T), we could only probe the first anomaly which involves transverse acoustic (TA) phonons with a lower sound velocity. The TA phonons follow the dispersion relation $\omega = v_T k$, where v_T is the TA phonon sound velocity. v_T is related to the elastic constant C_{44} and material density ρ by $C_{44} = \rho v_T^2$[49,50] and is determined to be 3968 m/s for NFO using $C_{44} = 82.3$ GPa and $\rho = 5230$ kg/m^3.[31,51]

We assume that magnons in NFO can also be described by a parabolic dispersion relation like for YIG ($\omega = \sqrt{(D_{ex}k^2 + \gamma\mu_0 H)(D_{ex}k^2 + \gamma(\mu_0 H + M_S))}$), where D_{ex} is the exchange stiffness, μ_0 the vacuum permeability, and γ the gyromagnetic ratio. From Fig. 1(b), we obtain M_S of our NFO sample to be 160 emu/cm^3 at room temperature, which equals 201 mT. The D_{ex} of NFO is not yet experimentally reported. In our experiment, from the peak positions observed at room temperature ($\mu_0 H_{TA} = \pm 4.0$ T), we can determine the only unknown parameter D_{ex} to be 5.5×10^{-6} m^2/s with both phonon and magnon dispersions. This value is close to D_{ex} which can be estimated from the exchange integrals among Ni^{2+}, Fe^{3+} (octahedral site), and Fe^{3+} (tetrahedral site).[52,53] Using the parameters given in Ref. 54, the D_{ex} of NFO can be estimated to be 6.4×10^{-6} m^2/s, within 17% difference of our experimental value.

Anomalies were also observed in the 450 nm NFO sample for electrically excited magnons in the field-sweep measurements of V_{EI} at $T = 150$ K, albeit with a lower signal-to-noise ratio. For the 40 nm NFO sample, however, no clear anomalies were identified in the measured range ($\mu_0 H \leq 6.6$ T) for V_{EI} or V_{TG}.

In summary, we have studied the magnon spin transport properties of epitaxial NFO films grown on MGO substrates in a nonlocal geometry. We obtained large nonlocal signals for both electrically and thermally excited magnons at short contact spacings, comparable to that of YIG. From the relaxation regime, λ_m was found to be around 2.5 μm. Furthermore, we observed anomalous features as a result of magnon-polarons formation in the field-dependent SSE measurements at both 150 and 293 K, from which the exchange stiffness constant of NFO can be determined. Our results demonstrate the improved quality of NFO grown on a lattice-matched substrate, showing NFO to be a potential alternative to YIG for spintronic applications. Specifically, both A and B sites of spinels can be versatilely substituted with other atoms at diverse composition ratios, allowing for more adaption and optimization of the material properties compared to garnets.

We thank Gerrit Bauer, Matthias Althammer, and Koichi Oyanagi for helpful discussions and would like to acknowledge M. de Roosz, H. Adema, T. Schouten, and J. G. Holstein for technical assistance. This work was supported by the research programs "Magnon Spintronics (Nr. 159)" and "Skyrmionics (Nr. 170)" of the Netherlands Organisation for Scientific Research (NWO), the NWO Spinoza prize awarded to Professor B. J. van Wees, DFG Priority Programme 1538 "Spin Caloric Transport" (KU 3271/1-1), NanoLab NL, EU FP7 ICT Grant No. InSpin 612759, and the Zernike Institute for Advanced Materials. The work at Alabama was supported by NSF Grant No. ECCS-1509875.

[1]A. V. Chumak, V. I. Vasyuchka, A. A. Serga, and B. Hillebrands, Nat. Phys. **11**, 453 (2015).
[2]L. J. Cornelissen, J. Liu, R. A. Duine, J. B. Youssef, and B. J. van Wees, Nat. Phys. **11**, 1022 (2015).
[3]S. T. B. Goennenwein, R. Schlitz, M. Pernpeintner, K. Ganzhorn, M. Althammer, R. Gross, and H. Huebl, Appl. Phys. Lett. **107**, 172405 (2015).
[4]J. Li, Y. Xu, M. Aldosary, C. Tang, Z. Lin, S. Zhang, R. Lake, and J. Shi, Nat. Commun. **7**, 10858 (2016).
[5]H. Wu, C. H. Wan, X. Zhang, Z. H. Yuan, Q. T. Zhang, J. Y. Qin, H. X. Wei, X. F. Han, and S. Zhang, Phys. Rev. B **93**, 060403 (2016).
[6]L. J. Cornelissen, K. J. H. Peters, G. E. W. Bauer, R. A. Duine, and B. J. van Wees, Phys. Rev. B **94**, 014412 (2016).
[7]M. Althammer, J. Phys. D: Appl. Phys. **51**, 313001 (2018).
[8]A. D. Karenowska, J. F. Gregg, V. S. Tiberkevich, A. N. Slavin, A. V. Chumak, A. A. Serga, and B. Hillebrands, Phys. Rev. Lett. **108**, 015505 (2012).
[9]T. Brächer, M. Fabre, T. Meyer, T. Fischer, S. Auffret, O. Boulle, U. Ebels, P. Pirro, and G. Gaudin, Nano Lett. **17**, 7234 (2017).
[10]K. Uchida, J. Xiao, H. Adachi, J. Ohe, S. Takahashi, J. Ieda, T. Ota, Y. Kajiwara, H. Umezawa, H. Kawai, G. E. W. Bauer, S. Maekawa, and E. Saitoh, Nat. Mater. **9**, 894 (2010).
[11]G. E. W. Bauer, E. Saitoh, and B. J. van Wees, Nat. Mater. **11**, 391 (2012).
[12]J. Xiao, G. E. W. Bauer, K.-c. Uchida, E. Saitoh, and S. Maekawa, Phys. Rev. B **81**, 214418 (2010).
[13]J. Shan, P. Bougiatioti, L. Liang, G. Reiss, T. Kuschel, and B. J. van Wees, Appl. Phys. Lett. **110**, 132406 (2017).

[14]R. Lebrun, A. Ross, S. A. Bender, A. Qaiumzadeh, L. Baldrati, J. Cramer, A. Brataas, R. A. Duine, and M. Kläui, Nature **561**, 222 (2018).
[15]C. Kittel, *Introduction to Solid State Physics*, 8th ed. (Wiley, Hoboken, NJ, 2004).
[16]H. Nakayama, M. Althammer, Y.-T. Chen, K. Uchida, Y. Kajiwara, D. Kikuchi, T. Ohtani, S. Geprägs, M. Opel, S. Takahashi, R. Gross, G. E. W. Bauer, S. T. B. Goennenwein, and E. Saitoh, Phys. Rev. Lett. **110**, 206601 (2013).
[17]M. Althammer, S. Meyer, H. Nakayama, M. Schreier, S. Altmannshofer, M. Weiler, H. Huebl, S. Geprägs, M. Opel, R. Gross, D. Meier, C. Klewe, T. Kuschel, J.-M. Schmalhorst, G. Reiss, L. Shen, A. Gupta, Y.-T. Chen, G. E. W. Bauer, E. Saitoh, and S. T. B. Goennenwein, Phys. Rev. B **87**, 224401 (2013).
[18]M. Isasa, A. Bedoya-Pinto, S. Vélez, F. Golmar, F. Sánchez, L. E. Hueso, J. Fontcuberta, and F. Casanova, Appl. Phys. Lett. **105**, 142402 (2014).
[19]M. Isasa, S. Vélez, E. Sagasta, A. Bedoya-Pinto, N. Dix, F. Sánchez, L. E. Hueso, J. Fontcuberta, and F. Casanova, Phys. Rev. Appl. **6**, 034007 (2016).
[20]Z. Ding, B. L. Chen, J. H. Liang, J. Zhu, J. X. Li, and Y. Z. Wu, Phys. Rev. B **90**, 134424 (2014).
[21]D. Meier, T. Kuschel, L. Shen, A. Gupta, T. Kikkawa, K. Uchida, E. Saitoh, J.-M. Schmalhorst, and G. Reiss, Phys. Rev. B **87**, 054421 (2013).
[22]E.-J. Guo, A. Herklotz, A. Kehlberger, J. Cramer, G. Jakob, and M. Kläui, Appl. Phys. Lett. **108**, 022403 (2016).
[23]T. Niizeki, T. Kikkawa, K-i Uchida, M. Oka, K. Z. Suzuki, H. Yanagihara, E. Kita, and E. Saitoh, AIP Adv. **5**, 053603 (2015).
[24]R. Ramos, T. Kikkawa, K. Uchida, H. Adachi, I. Lucas, M. H. Aguirre, P. Algarabel, L. Morellón, S. Maekawa, E. Saitoh, and M. R. Ibarra, Appl. Phys. Lett. **102**, 072413 (2013).
[25]K-i Uchida, T. Nonaka, T. Ota, and E. Saitoh, Appl. Phys. Lett. **97**, 262504 (2010).
[26]A. Aqeel, N. Vlietstra, J. A. Heuver, G. E. W. Bauer, B. Noheda, B. J. van Wees, and T. T. M. Palstra, Phys. Rev. B **92**, 224410 (2015).
[27]P. Bougiatioti, C. Klewe, D. Meier, O. Manos, O. Kuschel, J. Wollschläger, L. Bouchenoire, S. D. Brown, J.-M. Schmalhorst, G. Reiss, and T. Kuschel, Phys. Rev. Lett. **119**, 227205 (2017).
[28]T. Kuschel, C. Klewe, P. Bougiatioti, O. Kuschel, J. Wollschläger, L. Bouchenoire, S. D. Brown, J. M. Schmalhorst, D. Meier, and G. Reiss, IEEE Trans. Magn. **52**, 1 (2016).
[29]D. T. Margulies, F. T. Parker, M. L. Rudee, F. E. Spada, J. N. Chapman, P. R. Aitchison, and A. E. Berkowitz, Phys. Rev. Lett. **79**, 5162 (1997).
[30]A. V. Singh, B. Khodadadi, J. B. Mohammadi, S. Keshavarz, T. Mewes, D. S. Negi, R. Datta, Z. Galazka, R. Uecker, and A. Gupta, Adv. Mater. **29**, 1701222 (2017).
[31]A. Rastogi, A. V. Singh, Z. Li, T. Peters, P. Bougiatioti, D. Meier, J. B. Mohammadi, B. Khodadadi, T. Mewes, R. Mishra, J. Gazquez, A. Y. Borisevich, Z. Galazka, R. Uecker, G. Reiss, T. Kuschel, and A. Gupta, "Enhancement in Thermally Generated Spin Voltage at Nickel Ferrite/Pt Interface" (submitted).
[32]M. Schreier, N. Roschewsky, E. Dobler, S. Meyer, H. Huebl, R. Gross, and S. T. B. Goennenwein, Appl. Phys. Lett. **103**, 242404 (2013).
[33]N. Vlietstra, J. Shan, B. J. van Wees, M. Isasa, F. Casanova, and J. Ben Youssef, Phys. Rev. B **90**, 174436 (2014).
[34]J. Shan, L. J. Cornelissen, N. Vlietstra, J. Ben Youssef, T. Kuschel, R. A. Duine, and B. J. van Wees, Phys. Rev. B **94**, 174437 (2016).
[35]B. L. Giles, Z. Yang, J. S. Jamison, and R. C. Myers, Phys. Rev. B **92**, 224415 (2015).
[36]J. Shan, L. J. Cornelissen, J. Liu, J. B. Youssef, L. Liang, and B. J. van Wees, Phys. Rev. B **96**, 184427 (2017).
[37]B. L. Giles, Z. Yang, J. S. Jamison, J. M. Gomez-Perez, S. Vélez, L. E. Hueso, F. Casanova, and R. C. Myers, Phys. Rev. B **96**, 180412 (2017).
[38]L. J. Cornelissen, K. Oyanagi, T. Kikkawa, Z. Qiu, T. Kuschel, G. E. W. Bauer, B. J. van Wees, and E. Saitoh, Phys. Rev. B **96**, 104441 (2017).
[39]S. Vélez, V. N. Golovach, A. Bedoya-Pinto, M. Isasa, E. Sagasta, M. Abadia, C. Rogero, L. E. Hueso, F. S. Bergeret, and F. Casanova, Phys. Rev. Lett. **116**, 016603 (2016).
[40]N. Vlietstra, J. Shan, V. Castel, B. J. van Wees, and J. Ben Youssef, Phys. Rev. B **87**, 184421 (2013).
[41]Y.-T. Chen, S. Takahashi, H. Nakayama, M. Althammer, S. T. B. Goennenwein, E. Saitoh, and G. E. W. Bauer, Phys. Rev. B **87**, 144411 (2013).
[42]J. Liu, L. J. Cornelissen, J. Shan, T. Kuschel, and B. J. van Wees, Phys. Rev. B **95**, 140402 (2017).
[43]J. Liu, L. J. Cornelissen, J. Shan, B. J. van Wees, and T. Kuschel, J. Phys. D: Appl. Phys. **51**, 224005 (2018).
[44]R. A. Duine, A. Brataas, S. A. Bender, and Y. Tserkovnyak, *Universal Themes of Bose-Einstein Condensation*, edited by D. Snoke, N. Proukakis, and P. Littlewood (Cambridge University Press, Cambridge, United Kingdom, 2017), Chap. 26.
[45]T. Kikkawa, K. Shen, B. Flebus, R. A. Duine, K-i Uchida, Z. Qiu, G. E. W. Bauer, and E. Saitoh, Phys. Rev. Lett. **117**, 207203 (2016).
[46]B. Flebus, K. Shen, T. Kikkawa, K.-I. Uchida, Z. Qiu, E. Saitoh, R. A. Duine, and G. E. W. Bauer, Phys. Rev. B **95**, 144420 (2017).
[47]H. Man, Z. Shi, G. Xu, Y. Xu, X. Chen, S. Sullivan, J. Zhou, K. Xia, J. Shi, and P. Dai, Phys. Rev. B **96**, 100406 (2017).
[48]D. A. Bozhko, P. Clausen, G. A. Melkov, V. S. L'vov, A. Pomyalov, V. I. Vasyuchka, A. V. Chumak, B. Hillebrands, and A. A. Serga, Phys. Rev. Lett. **118**, 237201 (2017).
[49]H. Wang, D. Hou, T. Kikkawa, R. Ramos, K. Shen, Z. Qiu, Y. Chen, M. Umeda, Y. Shiomi, X. Jin, and E. Saitoh, Appl. Phys. Lett. **112**, 142406 (2018).
[50]O. Gülseren and R. E. Cohen, Phys. Rev. B **65**, 064103 (2002).
[51]Z. Li and E. S. Fisher, J. Mater. Sci. Lett. **9**, 759 (1990).
[52]C. M. Srivastava and R. Aiyar, J. Phys. C: Solid State Phys. **20**, 1119 (1987).
[53]A. Franco, H. V. S. Pessoni, and F. L. A. Machado, J. Appl. Phys. **118**, 173904 (2015).
[54]R. H. Kodama, A. E. Berkowitz, J. McNiff, E. J. McNiff, and S. Foner, Phys. Rev. Lett. **77**, 394 (1996).